

## RESULTS FROM THE ANALYSIS OF CRYSTAL BALL MESON PRODUCTION MEASUREMENTS AT BNL

R.A. Arndt, W.J. Briscoe, I.I. Strakovsky, and R.L. Workman

*Center for Nuclear Studies, Department of Physics  
The George Washington University, Washington, D.C. 20052*

The Crystal Ball spectrometer, with its nearly complete angular coverage, is an efficient detector of photon and neutron final states. While installed in the C6 beamline of the Alternating Gradient Synchrotron (AGS) of Brookhaven National Laboratory (BNL), this feature was used in a series of precise measurements of reactions with all-neutral final states. Here we concentrate on the analysis of data from the pion-induced reactions:  $\pi^- p \rightarrow \gamma n, \pi^0 n, \eta n$ , and  $\pi^0 \pi^0 n$ .

*Keywords:* resonances; scattering; detectors.

### 1. Overview

The Crystal Ball detector (Fig. 1), with its nearly  $4\pi$  angular coverage (94% of  $4\pi$ , utilizing 672 NaI crystals) is capable of measuring neutral final-state particles with high efficiency. The E913/E914 measurements reported here have provided very precise cross sections with broad angular coverage. Such data are invaluable for detailed partial-wave analyses. Below we consider how these data have impacted ongoing studies of the low-lying baryon resonances.

### 2. Charge-Exchange Reaction

Measurements of the charge-exchange reaction were made from threshold to  $T_{\pi^-} = 625$  MeV. Two regions were analyzed separately: the 64 to 212 MeV  $T_{\pi^-}$  range, dominated by the  $\Delta(1232)$  resonance <sup>1</sup>, and the 524 to 625 MeV range, which is clearly influenced by the opening  $\eta n$  channel <sup>2</sup>.

Agreement with an existing partial-wave solution (FA02 <sup>3</sup>) was found to be excellent. In fact the FA02 solution was often in better agreement with these new measurements than those originally included in the fit. The overall level of agreement with FA02 is illustrated in Fig. 2.

### 3. The Reaction $\pi^- p \rightarrow \eta n$

Differential cross sections for  $\eta n$  production were measured from threshold to  $T_{\pi^-} = 620$  MeV <sup>6</sup> with a goal to study the  $\eta n$  scattering length and  $\eta n$  couplings to the  $N(1535)$  and  $N(1520)$  resonances. The influence of this experiment is best illustrated in a plot comparing the Crystal Ball and prior measurements. In Fig. 3

## The Crystal Ball

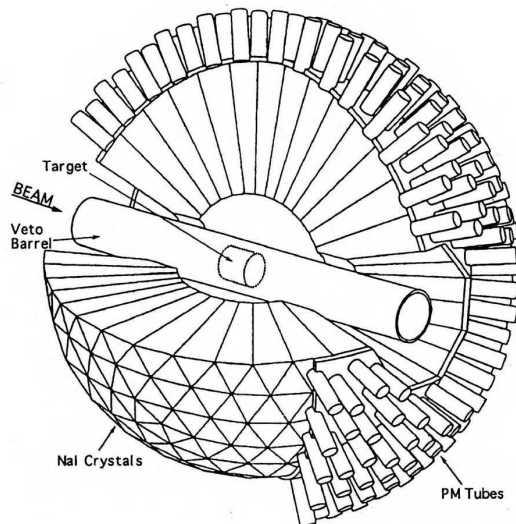


Fig. 1. Crystal Ball detector.

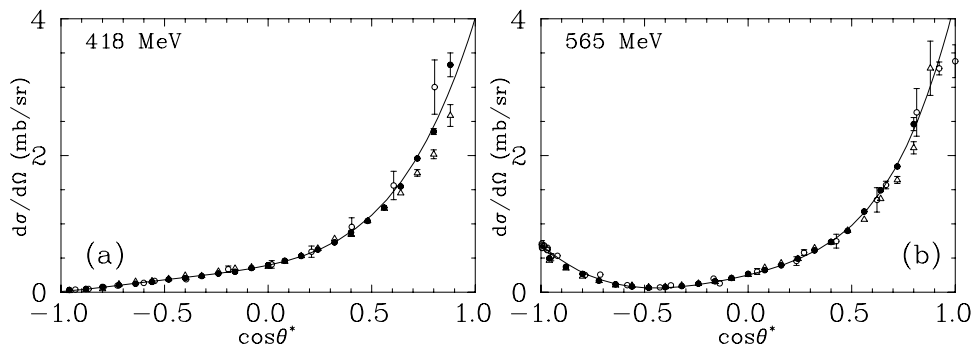


Fig. 2. Differential cross sections for  $\pi^- p \rightarrow \pi^0 n$ . The  $LH_2$  data (filled circles) are normalized to the central part of the  $CH_2$  spectra (open triangles). Solid lines show the FA02 predictions<sup>3</sup>. E913/E914 data are from Ref.<sup>4</sup>. Previous measurements<sup>5</sup> are shown as open circles.

we see how little the existing data contained single- and multi-channel fits to this reaction.

While the dominant contribution is S-wave, due to the  $N(1535)$  state, which decays mainly to  $\pi N$  and  $\eta N$ , the Crystal Ball data clearly reveal a small D-wave component, coming from the  $N(1520)$  resonance. This is made clear in Fig. 4, where we plot the coefficients of a Legendre polynomial expansion of the cross sections. Using a K-matrix fit to both the  $\pi N$  elastic scattering and  $\eta n$  production data, a  $N(1520)$   $\eta n$  branching fraction (0.08 to 0.16%) was extracted<sup>8</sup>.

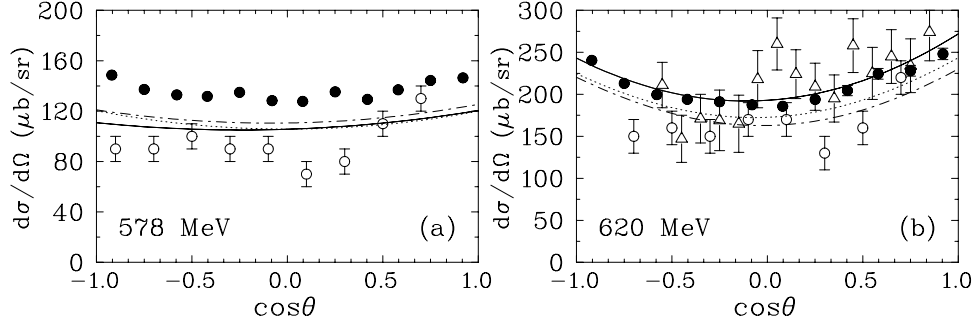


Fig. 3. Differential cross sections for  $\pi^- p \rightarrow \eta n$ . FA02<sup>3</sup> (E913/E914 data not included), G380, and Fit A<sup>8</sup> shown as solid, dash-dotted, and dotted lines, respectively. Experimental data are from<sup>6</sup> (filled circles),<sup>7</sup> (open circles), and<sup>5</sup> (open triangles) measurements.

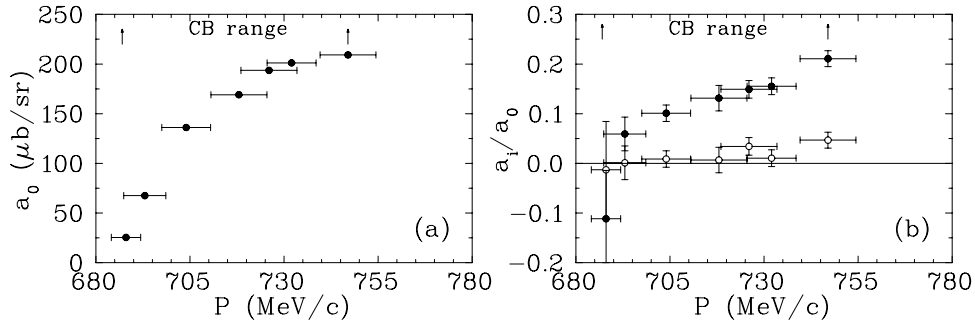


Fig. 4. Momentum dependency of (a) the  $a_0$  coefficient of a Legendre polynomial expansion of the differential cross sections and (b) ratio of the coefficients  $a_1/a_0$  (open symbol) and  $a_2/a_0$  (filled symbol). The horizontal errors include the  $\pm 2.5$  MeV/c beam momentum uncertainty and the beam momentum spread of E913/E914 data<sup>6</sup>.

A plot of  $\sigma^{\text{tot}}(\pi^- p \rightarrow \eta n)$  versus the eta-meson CM momentum ( $p_\eta^*$ ) is nearly linear to almost 200 MeV/c, due to the strong S-wave dominance. This is illustrated in Fig. 5. Both the Crystal Ball (solid points) and an earlier BNL measurement<sup>8</sup> (open circles) are consistent with linearity, though momentum uncertainty in the Crystal Ball experiment is magnified near threshold. Using the full near-threshold dataset, we extracted values for the  $\eta n$  scattering length,  $(1-1.15)+i(0.3-0.4)$  fm, reasonably consistent with the results of Green and Wycech<sup>9</sup> and Mosel<sup>10</sup>, if similar K-matrix methods were used. Rather different results followed from the use of a Chew-Mandelstam K-matrix.

Amplitude results using the Chew-Mandelstam K-matrix (G380) versus a K-matrix approach similar to that used in Ref.<sup>9</sup> (Fit A) are compared in Figs. 6–8. For the most important  $\pi N$  amplitudes,  $S_{11}$  and  $D_{13}$ , the differences are minor. Much larger deviations are seen in the amplitudes for  $\pi N \rightarrow \eta N$  and  $\eta N \rightarrow \eta N$ .

New results from a comprehensive partial-wave analysis of  $\pi^\pm p$  elastic scattering and charge-exchange data, covering the region from threshold to 2.6 GeV in the

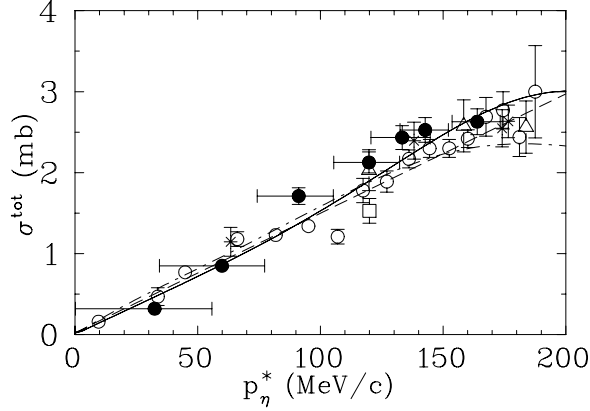


Fig. 5.  $p_\eta^*$  dependence of  $\sigma^{tot}(\pi^- p \rightarrow \eta n)$ . Data and notation given in Fig. 3. Dashed line shows a linear fit to E909 <sup>7</sup> (open circles) data.

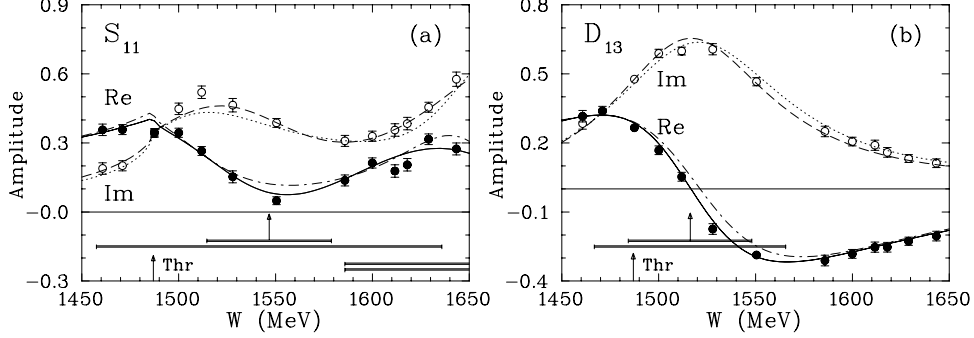


Fig. 6. (a)  $S_{11}$  and (b)  $D_{13}$  partial amplitudes for  $\pi N$  elastic scattering. Solid (dashed) curves give the real (imaginary) parts of amplitudes corresponding to the predictions of solution FA02 <sup>3</sup> (E913/E914 data not included). Single-energy solutions associated with FA02 are plotted as filled and open circles. Dash-dotted (dotted) curves show the real (imaginary) parts of amplitudes corresponding to G380. Differences between G380 and Fit A are not significant. All amplitudes are dimensionless. Vertical arrows indicate  $W_R$  and horizontal bars show full  $\Gamma/2$  and partial widths for  $\Gamma_{\pi N}$  associated with the FA02 results.

lab pion kinetic energy, employed a coupled-channel formalism to simultaneously fit  $\pi^- p \rightarrow \eta n$  data to 0.8 GeV <sup>16</sup>. This fit included all of the E913/E914 data mentioned above. Breit-Wigner parameters for resonances are listed in Table 1. In the SP06 and FA02 fits, a unitary Breit-Wigner plus background form was assumed for the resonant partial wave. Data within an energy bin were then fitted using this representation. The remaining waves were fixed to values found in the full global (SP06) analysis.

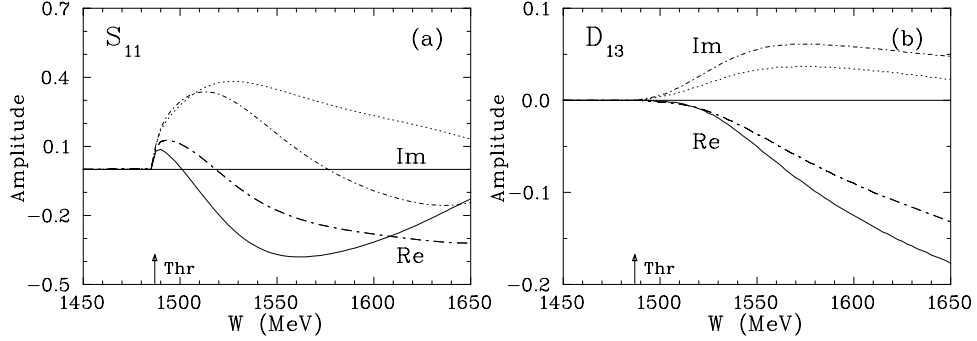


Fig. 7. (a)  $S_{11}$  and (b)  $D_{13}$  partial amplitude for  $\pi^- p \rightarrow \eta n$ . Dash-dotted (dotted) curves show the real (imaginary) parts of amplitudes corresponding to G380. Solid (short-dash-dotted) lines represent the real (imaginary) parts of amplitudes corresponding to the Fit A.

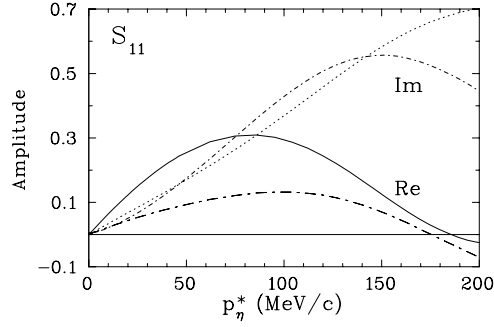


Fig. 8.  $p_\eta^*$  dependence of the  $S_{11}$  amplitude for the reaction  $\eta n \rightarrow \eta n$ . Dash-dotted (dotted) curves give the real (imaginary) parts of amplitudes corresponding to the solution G380. Solid (short-dash-dotted) lines represent the real (imaginary) parts of amplitudes Fit A.

#### 4. Inverse Pion Photoproduction

The inverse pion-photoproduction reaction ( $\pi^- p \rightarrow \gamma n$ ) has been measured at 18 values of  $T_{\pi^-}$  from 136 to 621 MeV<sup>4</sup>. Using detailed balance, these yield angular distributions for the photoproduction reaction ( $\gamma n \rightarrow \pi^- p$ ) for values of  $E_\gamma$  between 285 and 769 MeV, spanning the  $N(1440)$  resonance region. This procedure avoids the complication of extracting neutron-target information from the deuteron in a direct measurement of  $\pi^-$  photoproduction.

The Crystal Ball experiment has effectively doubled the  $\pi^-$  photoproduction database over the  $N(1440)$  region, and has been included in a modified multipole analysis. These new data were found to agree very well with predictions from the SAID and MAID multipole solutions. Only slight modifications of the SAID multipoles were required to obtain an overall  $\chi^2$  near unity for these data. A comparison with SAID and MAID results is interesting. In some cases, the predictions follow the Crystal Ball data while missing older measurements that were included in the SAID and MAID fits. An example is given in Fig. 9.

Table 1. Resonance couplings from a Breit-Wigner fit to the recent SP06<sup>16</sup>, our previous FA02<sup>3</sup> solutions, and a range from the [RPP]<sup>17</sup> (in square brackets). Masses  $W_R$ , widths  $\Gamma$ , and partial width  $\Gamma_{\pi N}/\Gamma$  are listed for isospin 1/2 baryon resonances relevant to the Crystal Ball measurements.

Resonance	$W_R$ (MeV)	$\Gamma$ (MeV)	$\Gamma_{\pi N}/\Gamma$	Ref
N(1440) $P_{11}$	1485.0±1.2	284±18	0.787±0.016	SP06
	1468.0±4.5	360±26	0.750±0.024	FA02
	[1420–1470]	[200–450]	[0.55–0.75]	RPP
N(1520) $D_{13}$	1514.5±0.2	103.6±0.4	0.632±0.001	SP06
	1516.3±0.8	98.6±2.6	0.640±0.005	FA02
	[1515–1525]	[100–125]	[0.55–0.65]	RPP
N(1535) $S_{11}$	1547.0±0.7	188.4±3.8	0.355±0.002	SP06
	1546.7±2.2	178.0±11.6	0.360±0.009	FA02
	[1525–1545]	[125–175]	[0.35–0.55]	RPP

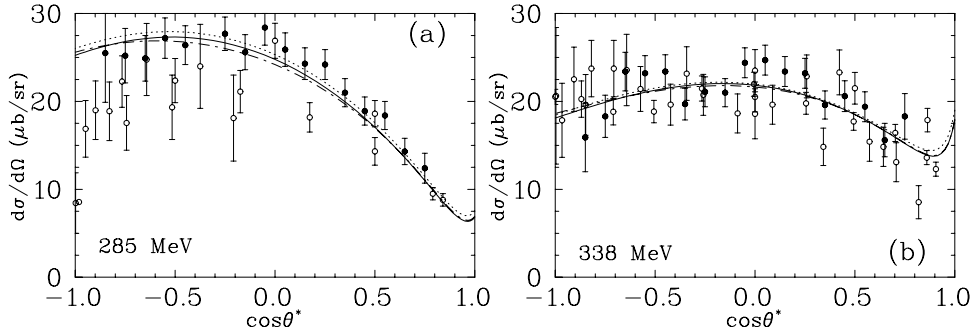


Fig. 9. Differential cross sections for  $\gamma n \rightarrow \pi^- p$ . Dashed-dotted (solid) curves correspond to SM02 (SH04) solution<sup>11</sup>. The MAID solution<sup>12</sup> are plotted with dashed lines. Experimental data are from E913/E914<sup>4</sup> (filled circles) and<sup>5</sup> (open circles) measurements.

## 5. The Reaction $\pi^- p \rightarrow \pi^0 \pi^0 n$

Measurements of the reaction  $\pi^- p \rightarrow \pi^0 \pi^0 n$  were made from 160 MeV, just above threshold, to 625 MeV<sup>13</sup>. The resulting total cross sections confirmed the trend found in an earlier near-threshold experiment<sup>14</sup>. At higher energies, the Crystal Ball results are far more precise than any previous determination. These two kinematic ranges are displayed in Fig. 10.

Dalitz plots of the 3-body final state suggested the dominance of a  $\pi^0 \Delta^0$  intermediate state, formed through the sequential process

$$\pi^- p \rightarrow N^* \rightarrow \pi^0 \Delta^0(1232) \rightarrow \pi^0 \pi^0 n. \quad (1)$$

The contribution of another sequential process

$$\pi^- p \rightarrow N^* \rightarrow f_0(600)n \rightarrow \pi^0 \pi^0 n \quad (2)$$

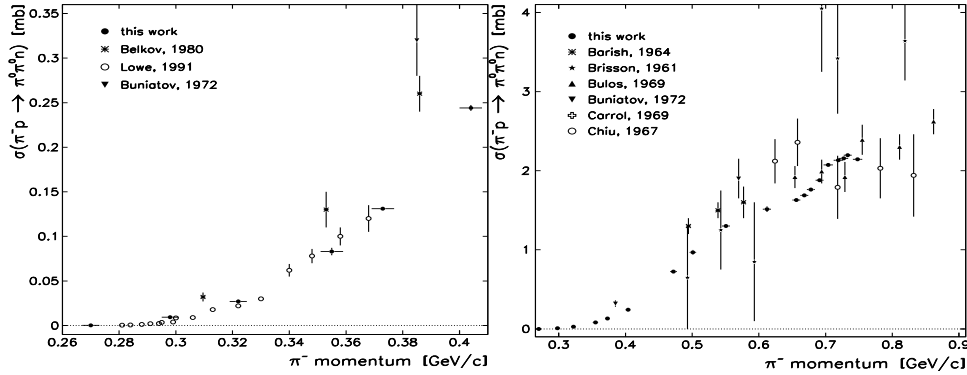


Fig. 10. Total cross sections for the  $\pi^- p \rightarrow \pi^0 \pi^0 n$  reaction. Experimental data are from E913/E914 <sup>13</sup> (filled circles) and previous <sup>13</sup> measurements.

was also considered. (The  $f_0(600)$  is a PDG designation for the more commonly known  $\sigma$  meson.) No direct evidence was found for this contribution, suggesting the need for a more detailed partial-wave analysis.

A number of recent calculations <sup>15</sup> have incorporated these measurements. Approaches explicitly including resonance contributions (the HB $\chi$ PT calculation did not), found important contributions from both of the above processes, with the most significant  $N^*$  being the  $N(1440)$  state.

## 6. The Future - the Crystal Ball and TAPS at MAMI

A program of photonuclear physics is in progress using the combination of the  $4\pi$  Crystal Ball and TAPS (Fig. 11) at MAMI. The facilities at MAMI include tagged, polarized photons and polarized  $p$ ,  $d$ , and  $^3He$  targets. Such a high-powered facility allows us to measure meson photoproduction and a variety of double polarization observables. The ‘‘Crystal Ball at MAMI’’ is now a top priority of the laboratory.

The combination of tagged photons and the Crystal Ball and TAPS provides an excellent opportunity for outstanding physics. MAMI B produces photons up to 800 MeV in 2-MeV bins. The MAMI C will provide photons up to 1400 MeV. The TAPS detector acting as the forward detection array of the CB, substantially improving the acceptance at forward angles. This provides almost- $4\pi$  coverage and a unique opportunity to measure reactions in which one or more of the final-state particles decay into photons. The Crystal Ball and TAPS also have a high detection efficiency for neutrons. This, coupled with the excellent energy resolution of the MAMI tagged photon beam, provides an opportunity to make precision measurements of the heretofore sparsely-measured neutral photoproduction channels.

## Acknowledgments

This work was supported in part by the U.S. Department of Energy grant DE-FG02-99ER41110 and by funding from Jefferson Lab.

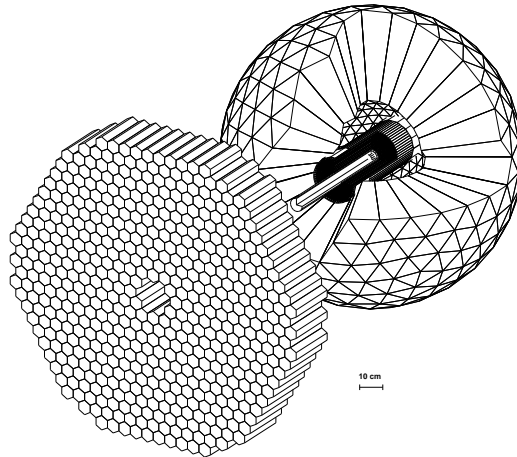


Fig. 11. The experimental apparatus for our measurements at MAMI. To show the position of the cylindrical wire chamber and the target inside the Crystal Ball some of the Crystal Ball crystals have been omitted.

## References

1. M.E. Sadler *et al.* [Crystal Ball Collaboration], *Phys. Rev. C* **69**, 055206 (2004).
2. A. Starostin *et al.* [Crystal Ball Collaboration], *Phys. Rev. C* **72**, 015205 (2005).
3. R.A. Arndt, W.J. Briscoe, I.I. Strakovsky, R.L. Workman, and M.M. Pavan, *Phys. Rev. C* **69**, 035213 (2004); SAID solutions at <http://gwdac.phys.gwu.edu>.
4. A. Shafi *et al.* [Crystal Ball Collaboration], *Phys. Rev. C* **70**, 035204 (2004).
5. The full database and numerous PWAs can be accessed via an ssh call to the SAID facility [gwdac.phys.gwu.edu](http://gwdac.phys.gwu.edu), with userid: said (no password), or a link to the website <http://gwdac.phys.gwu.edu>.
6. S. Prakov *et al.* [Crystal Ball Collaboration], *Phys. Rev. C* **72**, 015203 (2005).
7. T. W. Morrison *et al.*, *Bull. Am. Phys. Soc.* **45**, 58 (2000); T.W. Morrison, Ph. D. Thesis, The George Washington University, Dec. 1999.
8. R.A. Arndt, W.J. Briscoe, T.W. Morrison, I.I. Strakovsky, R.L. Workman, and A.B. Gridnev *Phys. Rev. C* **72**, 045202 (2005).
9. A.M. Green and S. Wycech, *Phys. Rev. C* **71**, 014001 (2005).
10. G. Penner and U. Mosel, *Phys. Rev. C* **66**, 055211 (2002).
11. R.A. Arndt, W.J. Briscoe, I.I. Strakovsky, and R.L. Workman, *Phys. Rev. C* **66**, 055213 (2002).
12. D. Drechsel, O. Hanstein, S.S. Kamalov, and L. Tiator, *Nucl. Phys.* **A645**, 45 (1999).
13. S. Prakov *et al.* [Crystal Ball Collaboration], *Phys. Rev. C* **69**, 045202 (2005).
14. J. Lowe *et al.* *Phys. Rev. C* **44**, 956 (1991).
15. N. Mobed, J. Zhang, and D. Singh, *Phys. Rev. C* **72**, 045204 (2005); H. Kamano and M. Arima, *Phys. Rev. C* **73**, 055203 (2006); S. Schneider, S. Krewald, and Ulf-G. Meissner, [nucl-th/06030](http://nucl-th/06030).
16. R.A. Arndt, W.J. Briscoe, I.I. Strakovsky, and R.L. Workman, 'Extended partial-wave analysis of  $\pi N$  scattering data,' submitted to *Phys. Rev. C* [[nucl-th/0605082](http://nucl-th/0605082)].
17. S. Eidelman *et al.*, *Review of Particle Physics*, *Phys. Lett. B* **592**, 1 (2004).